

FOUNDATIONS OF LARGE LANGUAGE MODEL COMPRESSION—PART 1: WEIGHT QUANTIZATION

Sean I. Young

siyoung@csail.mit.edu

ABSTRACT

In recent years, compression of large language models (LLMs) has emerged as an important problem to enable language model deployment on resource-constrained devices, reduce computational costs, and mitigate the environmental footprint of large-scale AI infrastructure. In this paper, we lay down the foundation for LLM quantization from a convex optimization perspective and propose a quantization technique that builds on this foundation for optimum quantization outcomes. Our quantization framework, CVXQ, scales to models containing hundreds of billions of weight parameters and provides users with the flexibility to compress models to any specified model size, post-training. A reference implementation of CVXQ can be obtained from github.com/seannz/cvxq.

1 INTRODUCTION

Large language Models (LLMs) have become a versatile framework for solving a large number of problems in natural language processing, from text translation and summarization to conversational AI and automatic generation of radiologists’ reports. While LLMs have surpassed traditional methods in many of these tasks, they can involve tens or hundreds of billions of weight parameters (!), and this makes their deployment onto devices with limited resources challenging—model weights and activations far exceed the available device memory so that activations need to be loaded from and saved to off-chip memory throughout inference, rendering LLM inference memory-bound (Yuan et al., 2024). This greatly hinders the usability of LLMs particularly in time-sensitive applications and exacerbates the environmental footprint of large-scale AI infrastructure required by LLMs.

One way to reduce the memory requirements of large models for inference is by compressing (that is, simplifying) the representation of the model weights and activations after training. This can be achieved via weight pruning, quantization of activations and weights, or PCA-type dimensionality reduction of weight matrices. Out of these, quantization of weights and activation has proven to be particularly useful for compressing models to very low bit depths or arbitrary user-specified model sizes (Dettmers et al., 2022; Yao et al., 2022; Frantar et al., 2022; Frantar & Alistarh, 2022; Lin et al., 2024; Kim et al., 2024; Shao et al., 2024; Lee et al., 2024; Guan et al., 2024). Using state-of-the-art quantization techniques, it is now possible to compress 10–100 billion-parameter LLMs to four bits per weight on average with negligible loss of model accuracy (Frantar et al., 2022; Lin et al., 2024), facilitating LLM inference on a single consumer-grade GPU for example.

Although significant advances have been made in LLM quantization recently, current approaches to model quantization still lead to considerably reduced model accuracy at low bit depths, with many methods fine-tuning model weights during quantization (Frantar et al., 2022; Lee et al., 2024). This makes such quantization methods unsuited to the quantization of activations during inference, where fine-tuning the values of activations would lead to unacceptable delays in the inference pipeline.

Given the symmetry between weights and hidden states in matrix multiplications, achieving fast and accurate quantization of both weights and activations can be crucial for enhancing computational efficiency and prediction accuracy of LLMs, as well as for informing hardware design. This work aims to address gaps in the current model compression literature and advance compression methods further to enable accurate and efficient inference on quantized LLMs.

In this paper—the first of a three-part series—we tackle the problem of LLM compression using the

framework of convex optimization. We begin with the problem of weight quantization and analyze how a model’s weights should be quantized to maximize quantized model accuracy for a given bit size. We then propose a stochastic gradient descent-type algorithm to solve this problem exactly and efficiently, post-training—in minutes for billion-parameter models and in a few hours for 10–100-billion-parameter models. Compared with the recent OPTQ family of quantization methods (Frantar et al., 2022; Frantar & Alistarh, 2022; Huang et al., 2024; Lee et al., 2024), which fine-tune weights during quantization, our approach spends almost zero time on actual quantization once the optimal bit depths have been determined. This makes our framework also suited to quantizing intermediate activations, which can further reduce the memory footprint of LLM inference. Part 2: Activation Quantization discusses this and other hardware aspects of quantization in detail.

2 PREVIOUS WORK

Early work on neural network model quantization can be attributed to Vanhoucke et al. (2011), who demonstrated that 8-bit integer arithmetic can be used for network training and inference without incurring a significant loss of accuracy. More generally, quantization-aware training (QAT) (Zhou et al., 2017; Jacob et al., 2018; D. Zhang et al., 2018; Esser et al., 2019; Y. Choi et al., 2017; Wang et al., 2019) integrates the quantization process into training by allowing the model to adapt to the reduced precision in weights (Esser et al., 2019; Jacob et al., 2018; D. Zhang et al., 2018; Zhou et al., 2017) and activations (Y. Choi et al., 2017; Wang et al., 2019) by determining the optimum bit depth (Wang et al., 2019; D. Zhang et al., 2018) and step size (Esser et al., 2019) using back-prop to facilitate the gradient to flow through quantization operators. One shortcoming of QAT methods is that model training needs to be repeated for different quantized model sizes and accuracy, which makes them less suitable for quantizing larger models that require substantial computation and time for training.

More recent quantization techniques for language and vision models aim to facilitate compression of already trained models for rapid deployment without further training (Dong et al., 2019; Chen et al., 2021; Dettmers et al., 2022; Yao et al., 2022; Frantar et al., 2022; Dettmers et al., 2023; Xiao et al., 2023; Lin et al., 2024; Kim et al., 2024; Shao et al., 2024; Lee et al., 2024). These approaches quantize model weights to 3–4 or 8 bits for integer-arithmetic-only inference (Jacob et al., 2018) using mixed bit depth quantization (Wang et al., 2019; Chen et al., 2021) or by a separate handling of outlier channels (Zhao et al., 2019) to improve the accuracy of the quantized model. Loss-aware quantization techniques (Hou & Kwok, 2018; Nahshan et al., 2020; Qu et al., 2020) seek to minimize accuracy loss in quantized models by calibrating quantization and biases on calibration data. Data-free quantization methods (Nagel et al., 2019; Xu et al., 2020; K. Choi et al., 2021; Qian et al., 2023) attempt to remove the need for real calibration data by matching the distribution of weights instead (Nagel et al., 2019) or using synthetic data in place of real calibration data (K. Choi et al., 2021).

For LLM compression in particular, an extension to the Optimum Brain Surgeon (OBS) algorithm (Hassibi & Stork, 1992) known as GPTQ (Frantar et al., 2022) was proposed for the quantization of 1–100 billion parameter models. Further recent extensions to GPTQ (Dettmers et al., 2023; Lee et al., 2024) optionally incorporate the handling of sensitive weights by scaling or simply by retaining the original weight values, with other approaches (Lin et al., 2024; Xiao et al., 2023) independently incorporating similar ideas. Later, we will see that our convex optimization formulation provides a disciplined approach to incorporating channel sensitivity for mixed precision weight quantization.

3 QUANTIZATION FRAMEWORK

Here, we use the task of next-token prediction in language modeling as a running example. For our purposes, the end-to-end mapping of input token embeddings to predicted next-token embeddings by a pretrained language model f can be expressed in the most general form as

$$\mathbf{Z} = f(\mathbf{X}) = f(\mathbf{X}, \Theta_1, \Theta_2, \dots, \Theta_N) = f(\mathbf{X}, \Theta_1, \Theta_2, \dots, \Theta_N, \mathbf{B}_1, \mathbf{B}_2, \dots, \mathbf{B}_N) \quad (1)$$

in which $\mathbf{X} \in \mathbb{R}^{L \times E}$ denotes a sequence of L tokens, each of which resides in some E -dimensional embedding space, and $\mathbf{Z} \in \mathbb{R}^{L \times E}$, embeddings of L predicted next tokens. The m th block of weight matrices $\Theta_{mM+1}, \dots, \Theta_{(m+1)M}$ and bias vectors $\mathbf{B}_{mM+1}, \dots, \mathbf{B}_{(m+1)M}$ jointly parameterize the m th transformer block, which refines the embeddings produced by the $(m - 1)$ th transformer block. In

Algorithm 1. CVXQ: Convex Optimization for Weight Quantization

```

1 Input:  $f(\cdot, \Theta_1, \dots, \Theta_N)$  (model),  $\{\mathbf{X}\}$  (calibration set),  $R$  (target bit rate),  $B_{\max}$  (max bit depth)
2 Output:  $B_1, \dots, B_N$  (bit depths),  $S_1, \dots, S_N$  (weight scales),  $\mu_1, \dots, \mu_N$  (weight means)
3 Initialize:  $\mathbf{U} \leftarrow \text{pca\_basis}(\{\mathbf{X}\}) \in \mathbb{R}^{E \times E}$ ,  $\mathbf{S} \leftarrow \text{sub\_sample}(\mathbf{I}_{L \times L}) \in \mathbb{R}^{L \times L}$ ,  $V \leftarrow 10^{-6}$ 
4    $B_n \leftarrow \infty$ ,  $G_n^2 \leftarrow 0$ ,  $\mu_n \leftarrow \text{mean}(\Theta_n)$ ,  $S_n \leftarrow \text{std}(\Theta_n)$ ,  $\Theta_n^q \leftarrow \Theta_n$ ,  $B_n^q \leftarrow B_n$ ,  $\bar{\mathbf{X}}_n \leftarrow \mathbf{0}$  for  $n$  in  $1, \dots, N$ 
5 for iter in  $1, \dots, \text{max\_iter}$  do
6   for  $\mathbf{X}$  in minibatch do
7      $\mathbf{Z}, \mathbf{X}_1, \dots, \mathbf{X}_N \leftarrow f(\mathbf{X}, \Theta_1^q, \dots, \Theta_N^q, B_1^q, \dots, B_N^q)$ 
8      $\bar{\mathbf{X}}_n \leftarrow (1 - \alpha)\bar{\mathbf{X}}_n + (\alpha/L)\mathbf{1}^T \mathbf{X}_n$  for  $n$  in  $1, \dots, N$ 
9      $\Gamma_1, \dots, \Gamma_N \leftarrow \text{autograd}(\mathbf{S}^T \mathbf{Z} \mathbf{U}, \Theta_1^q, \dots, \Theta_N^q)$ 
10     $G_n^2 \leftarrow (1 - \alpha)G_n^2 + (\alpha/P_n) \text{trace}(\Gamma_n^T \Gamma_n)$  for  $n$  in  $1, \dots, N$ 
11    for  $_$  in  $1, \dots, 10$  do
12       $B_n \leftarrow \text{clamp}(\frac{1}{2} \log_2(G_n^2 S_n^2 / V), 0, B_{\max})$  for  $n$  in  $1, \dots, N$ 
13       $V \leftarrow V + \beta(\text{sum}(P_n B_n) - (\text{sum}(P_n))R)$ 
14     $\Theta_n^q \leftarrow \text{compand\_quantize}(\Theta_n, B_n, S_n, \mu_n)$ ,  $B_n^q \leftarrow B_n + (\Theta_n^q - \Theta_n)\bar{\mathbf{X}}_n$  for  $n$  in  $1, \dots, N$ 

```

practice, LLM frameworks used in language modeling also require an embedder $\Theta_0 \in \mathbb{R}^{E \times V}$ and a prediction head $\Theta_{N+1} \in \mathbb{R}^{V \times E}$ to transform between embeddings and tokens from a vocabulary of size V , but for now, we focus on the compression of transformer block weights as is typically done in model weight quantization work (Frantar et al., 2022; Lee et al., 2024; Lin et al., 2024).

To get a sense of the number of weight matrices and their sizes in a typical language model, the 13 billion-parameter model in the OPT family (OPT-13B) contains $N = 240$ weight matrices in blocks of $M = 6$, with each block comprising $12E^2$ weights in an embedding dimension of $E = 5120$. The embedder and prediction head are parameterized by a shared matrix containing VE weights, where the vocabulary size $V = 50272$. Note that each transformer block also contains $9E$ bias parameters but due to their relative scarcity, bias parameters can be communicated losslessly and still have little to no impact on the overall compression performance (Frantar et al., 2022).

Notionally, the elements of a weight matrix Θ are continuously valued so they require quantization for efficient communication and storage. Compared with vector and lattice quantization techniques (Egiazarian et al., 2024; Gong et al., 2015), scalar quantization (Frantar et al., 2022; Lin et al., 2024) can simplify decoding and even enable operations directly on quantization indices, which obviates the need for a separate dequantization process. The mid-rise uniform scalar quantization of a weight θ at a bit-depth of B bits and step size D can be expressed as

$$\theta^q(B, D) = D(\text{clip}(\text{floor}(D^{-1}\theta), -2^{B-1}, 2^{B-1} - 1) + 2^{-1}), \quad B = 0, 1, 2, \dots \quad (2)$$

and $\theta^q(B, D) = \theta$ if $B = \infty$ (for notational convenience). The problem of compressing a model f now amounts to determining the optimal bit depth B and the associated quantization step size D for model weights. It would be impractical, however, to determine a separate (B, D) for each weight θ in the model since the cost of signaling the choice of (B, D) for each one would far outweigh the bit savings derived from quantization. Typically, a single (B, D) pair is used to quantize a small group of weights (an entire matrix or rows or columns thereof) in which case the cost of signaling (B, D) can be borne by a group of quantized weight parameters as a negligible per-weight overhead.

3.1 BIT DEPTH ASSIGNMENT

Suppose we want to compress f by quantizing each matrix Θ_n containing P_n elements according to its own bit depth B_n and step size $D_n^*(B_n)$. How should B_n be decided? Roughly speaking, weights that are more sensitive to output distortion should be allotted more bits to “balance the scales” while keeping the total number of bits under a given model bit budget. We can formalize this notion by expressing the weight quantization task at hand as a constrained non-linear least-squares problem:

$$\begin{aligned} & \text{minimize } d(B_1, \dots, B_N) = \mathbb{E}_{\mathbf{X}} \|f(\mathbf{X}, \Theta_1^q(B_1, D_1^*(B_1)), \dots, \Theta_N^q(B_N, D_N^*(B_N))) - f(\mathbf{X})\|_F^2 \\ & \text{subject to } r(B_1, \dots, B_N) = \sum_{n=1}^N P_n B_n - (\sum_{n=1}^N P_n) R = 0 \end{aligned} \quad (3)$$

in which R denotes a user-specified average model bit depth (bit rate). This problem is reminiscent of optimal resource allocation, where the objective is to maximize some utility (or minimize output

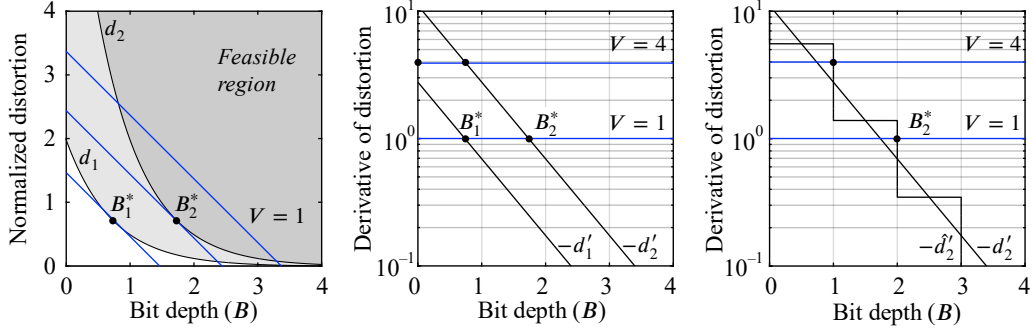


Figure 1: Optimal bit depths. Consider two weight matrices whose distortion functions are given by d_1 and d_2 , where $d_n(B_n) = G_n^2 S_n^2 2^{-2B_n}$. For any given value of the dual variable V , optimal bit depths B_1^* and B_2^* are found where the derivative of d_1 and d_2 is $-V$, respectively (left). These points correspond to the intersections between V and $-d'_n = (2 \ln 2) d_n$ (center). Integerized bit depths occur on the rounded curves $-d'_n$ (right).

distortion in our case) by optimally spending down a given budget (the total number of bits). In this section and next, we provide insights into problem (3) and discuss its solution; see Algorithm 1.

To apply the machinery of numerical optimization to (3), we will relax the discrete constraint on the bit depths B_1, \dots, B_N while solving the problem and round the solution B_1^*, \dots, B_N^* to the nearest integers after they have been obtained. Let us write the Lagrangian of (3) as $\mathcal{L}(B_1, \dots, B_N, V) = d(B_1, \dots, B_N) + Vr(B_1, \dots, B_N)$, where V is a dual variable associated with the equality constraint of (3). Setting to 0 the partials of \mathcal{L} with respect to B_1, \dots, B_N, V yields the optimality conditions

$$\frac{1}{P_1} \frac{\partial d(B_1, B_2, \dots, B_N)}{\partial B_1} = \dots = \frac{1}{P_N} \frac{\partial d(B_1, B_2, \dots, B_N)}{\partial B_N} = -V, \quad r(B_1, \dots, B_N) = 0 \quad (4)$$

so, problem (3) can be solved by alternately updating the bit depths B_1, \dots, B_N (primal variables) and the trade-off V (dual variable) until all optimality conditions are met. In words, the optimality conditions are reached once the marginal decrease in the output distortion from an infinitesimal bit is equal across layers at $-V$ and once we have assigned exactly R bits per weight on average.

Since the quantization function (2) is constant almost everywhere, a naive computation of the partial derivatives of d with respect to B_1, \dots, B_N using the chain rule of differentiation does not provide a useful direction for descent. One result from rate–distortion theory (Gersho & Gray, 1991) is that for any random variable of finite variance, quantization error decreases by half with every additional bit at a sufficiently high bit depth. More specifically to our problem, we can write (Appendix A)

$$-\frac{1}{2 \ln 2} \frac{\partial d(B_1, \dots, B_N)}{\partial B_n} \approx \mathbb{E}_X \left\| \frac{\partial f(\Theta_1^q(B_1), \dots, \Theta_N^q(B_N))}{\partial \Theta_n} \Delta_n^q(B_n) \right\|_F^2 \approx P_n H_n \underbrace{G_n^2 S_n^2 2^{-2B_n}}_{= d_n(B_n)} \quad (5)$$

in which $\Theta_n^q(B_n) = \Theta_n^q(B_n, D_n^*(B_n))$ for brevity, G_n^2 and S_n^2 represent the variances of the elements of $\partial_{\Theta_n} f(\mathbf{X}, \Theta_1^q, \dots, \Theta_N^q)$, and of Θ_n^q , respectively, and H_n is a quantization coefficient that depends on the type of weight distribution, with $H_n = 1.42$ for Gaussian, 0.72 for Laplace, etc. (Gersho & Gray, 1991). Assuming weights are distributed similarly across layers with $H_1 = \dots = H_N$, factors H_n and constant $-\frac{1}{2 \ln 2}$ can be removed the above expression without affecting the solution of (3).

Coupled with the above closed-form expression for the partial derivatives, optimality conditions (4) naturally lend themselves to dual ascent-type methods for solving problem (3). The idea behind dual ascent (Boyd et al., 2011) is to alternately update the primal B_1, \dots, B_N , and dual V variables, with one set held fixed while updating the other. After initializing $B_1 = \dots = B_N = \infty$, V to some small positive number, and computing G_1^2, \dots, G_N^2 , we update the bit depths and trade-off iteratively via

$$B_n \leftarrow \text{clamp} \left(\frac{1}{2} \log_2 \left(\frac{G_n^2 S_n^2}{V} \right), 0, B_{\max} \right) \quad \text{for } n = 1, \dots, N \quad (6)$$

$$V \leftarrow V + \alpha \left(\sum_{n=1}^N P_n B_n - \left(\sum_{n=1}^N P_n \right) R \right)$$

in which α denotes a step size for dual update. Figure 1 illustrates the optimality conditions for bit

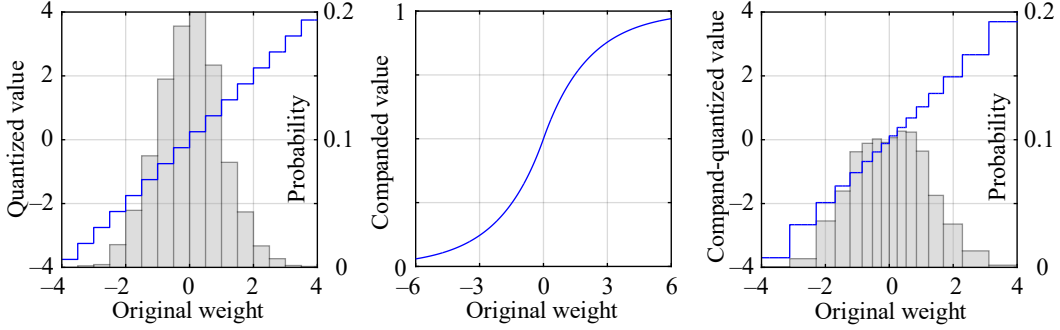


Figure 2: Companding quantization. Illustrated for a 4-bit quantizer (16 quantization levels) on Gaussian weights with zero mean and unit variance. Uniform quantization across the entire range of weight values (left) leads to unduly large quantization bins (hence quantization errors) for more probable weights. Companding the weights to the range (0,1) prior to uniform quantization (middle) reduces quantization errors for more probable weights (right), reducing the mean square error.

depths. With G_n^2 and S_n^2 fixed, dual ascent steps (6) typically converge within a few iterations (tol = 10^{-6} bit, step size $\alpha = 2$) after which the obtained B_n are rounded to integers. The non-linear nature of the least squares objective d (3) means that iteration (6) should be repeated after the bit depths B_n are updated. Using the updated B_n , we first obtain the re-quantized weights $\Theta_n^q(B_n)$ along with the re-computed gradient variances G_n^2 , based on which B_n can be further updated via (6).

Evaluating $\partial_{\Theta_n} f(\mathbf{X}, \Theta_1^q(B_1), \dots, \Theta_N^q(B_N))$ across the entire calibration set at every iteration is prohibitively expensive given the dimensionality of the output $f(\mathbf{X}) \in \mathbb{R}^{L \times E}$ and the cost of back-propagating each element through f . To overcome this difficulty, we perform PCA on $f(\mathbf{X})$ along the embedding dimension (of E) and sub-sample along the token dimension (of T), and accumulate gradient variances by back-propagating only a mini-batch of calibration examples every time:

$$G_n^2 \leftarrow (1 - \beta)G_n^2 + \beta \mathbb{E}_{\mathbf{X} \sim \text{batch}} \left\| \frac{\partial \mathbf{S}^T f(\Theta_1^q(B_1), \dots, \Theta_N^q(B_N)) \mathbf{U}}{\partial \Theta_n} \right\|_F^2 \quad \text{for } n = 1, \dots, N \quad (7)$$

in which β denotes the learning rate, and \mathbf{S}^T and \mathbf{U} represent the PCA projection and sub-sampling operators, respectively. In practice, we further accelerate variance accumulation by cycling through PCA coefficients and back-propagating only one coefficient per sample in every minibatch.

3.2 STEP SIZES AND BIASES

Suppose now the weight matrices $\Theta_1, \dots, \Theta_N$ are to be assigned bit depths B_1, \dots, B_N (which are not necessarily optimum.) We now investigate how the quantization step size D_n should be decided given bit depth B_n . In the round-to-nearest scheme (RTN, Figure 2, left), D_n is always chosen such that the quantizer's 2^{B_n} steps just cover the entire range of weight values, and this step size halves as B_n is increased by one. These criteria optimize step sizes when weights are distributed uniformly across a range and the objective is to minimize distortion in quantized weights.

For LLMs, the elements θ of a weight matrix typically exhibit a light-tailed distribution p_θ (normal or Laplace) (Zhao et al., 2019), which renders partitioning the entire weight range into 2^{B_n} equal steps sub-optimal especially at low bit depths (Cover & Thomas, 2006; Gersho & Gray, 1991). One alternative to the computationally expensive Lloyd–Max algorithm (Lloyd, 1982; Max, 1960) is companded quantization (Gray & Neuhoff, 1998), which applies a sigmoid transform to θ prior to uniform quantization to achieve finer quantization in regions of larger p_θ and coarser quantization in regions where is smaller p_θ ; see Figure 2 (right). When the weights θ are Laplace-distributed with mean μ and variance S^2 , an asymptotically optimal choice of sigmoid function is (Appendix B):

$$\sigma(\theta, S, \mu) = \frac{1 + \text{sgn}(\theta - \mu)}{2} \exp\left(-\frac{\sqrt{2} \text{abs}(\theta - \mu)}{3S}\right) \in (0, 1), \quad \theta \in (-\infty, \infty), \quad (8)$$

that is, the normalized cubic root of the cumulative distribution function for a Laplace distribution of the same mean and variance. Companded weights $\theta^\sigma = \sigma(\theta, S, \mu)$ are then quantized uniformly

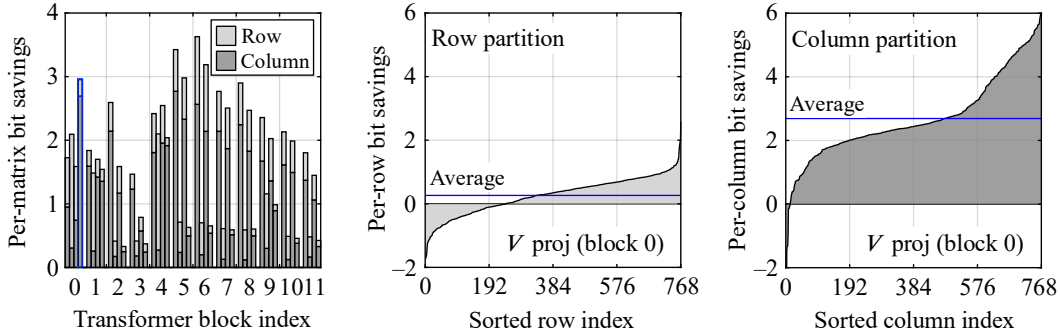


Figure 3: Bit savings from partition. Plotted for OPT-125m. Savings are derived by partitioning each weight matrix into a collection of row or column matrices and assigning each sub-matrix its own bit depth. Savings differ across the (Q , K , V and O) projection matrices of the model’s 12 transformer blocks (left). Per-column (middle) and row (right) bit savings (shown for block 3, O -proj) can dip below zero but are always positive on average due to Jensen’s inequality (see text).

in the range (0, 1) and signaled together with the bit depth B and scale S for efficient dequantization using lookup tables. In practice, S, μ are treated as hyper-parameters and fine-tuned efficiently on coarse 1D grids as a post-processing step (Young et al., 2021) once Algorithm 1 has completed.

Quantization invariably causes small deterministic differences to arise between the original (non-quantized) Θ and quantized Θ^q weights. While these errors are often modeled as zero-mean noise in theoretical analyses, they are seldom zero-mean in practice and can lead to systematically biased model output, which significantly reduces prediction accuracy. To compensate for these non-zero differences, we compute new bias vectors for the model as $\mathbf{B}_n^q \leftarrow \mathbf{B}_n + (\Theta_n^q - \Theta_n) \bar{\mathbf{X}}_n$ each time the matrix Θ_n is quantized. Here, $\bar{\mathbf{X}}_n$ is a vector of running means of the inputs to the n th layer, which is accumulated during the forward pass in a manner analogous to the accumulation of G_n^2 during the backward pass. The corrected biases \mathbf{B}_n^q are then used whenever the corresponding quantized weight matrices Θ_n^q are used during gradient variance accumulation and inference.

3.3 MATRIX PARTITIONING

Rather than quantize optimally at the granularity of a whole weight matrix, we can split each matrix into a collection of row or column matrices, assigning optimum bit depth and step size to each sub-matrix. In this case, the total number of matrices N in (3) can be reinterpreted as the total number of sub-matrices collected across all layers, with the quantities B_n , D_n and P_n , similarly interpreted as the bit-depth, step size and number of elements of the n th sub-matrix. Note that quantizing at the granularity of row or column sub-matrices does not noticeably increase the complexity of variance accumulation, as the same squared gradients computed via back-propagation can be averaged per sub-matrix to produce the corresponding sub-matrix variances. Here, without loss of generality, we assume that each matrix is split into a collection of column matrices.

For a weight matrix Θ with gradient and weight variances G^2 and S^2 , whose per-column variances are G_1^2, \dots, G_N^2 and S_1^2, \dots, S_N^2 , respectively, the theoretical gain (average bit depth savings) from partitioning can be expressed as

$$\gamma_{\text{partition}} = \frac{1}{2} \left(\log_2(G^2 S^2) - \frac{1}{N} \sum_{n=1}^N \log_2(G_n^2 S_n^2) \right), \quad (9)$$

a non-negative quantity as a direct result of Jensen’s inequality. This quantity represents the bit-rate (average bit-depth) savings when the n th column is assigned $B_n = \frac{1}{2} \log_2(G_n^2 S_n^2) + B$ bits for some B , compared to assigning a uniform bit depth $B_n = \frac{1}{2} \log_2(G^2 S^2) + B$ bits across all columns under the assumption that the weights of its N columns are identically distributed. Figure 3 (left) plots the per-matrix bit-depth savings derived by partitioning the (Q , K , V and O) projection matrices of the OPT-125m model by rows or columns. The per-channel breakdown of the savings is also shown.

In addition to primary splitting of matrices into columns, we may want to further split each column into a fixed number of groups of weight elements given the presence of row bit savings as well. To split the columns of a weight matrix $\Theta \in \mathbb{R}^{N \times N}$, one can simply cluster its rows into M similarly

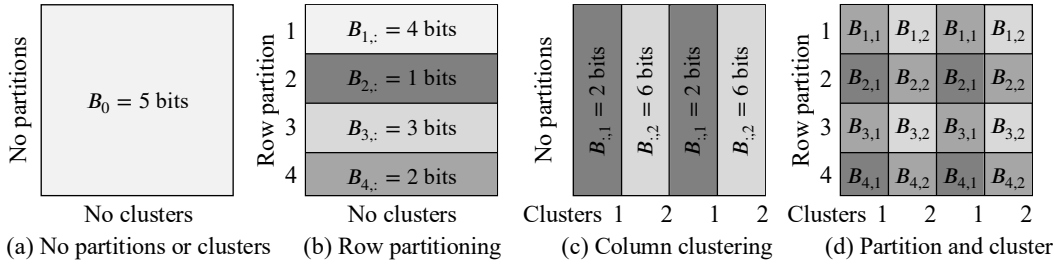


Figure 4: Partitioning and clustering. Illustrated for a 4×4 weight matrix. Rather than assign the same bit depth to all elements of a weight matrix (a), we can assign a separate bit depth to each row of weights (b), or to a cluster of columns (c), and even combine partitioning and clustering (d) to realize row- and column-based bit savings.

sized groups based on their row variances $G_1^2 S_1^2, \dots, G_N^2 S_N^2$. By applying the same clustering to all columns of a matrix, we can signal the cluster index for each row using $\lceil \log_2 M \rceil$ bits—a negligible per-weight overhead for a typical number of columns in a large matrix and the number of groups used in practice. We illustrate partitioning and subdivision in Figure 4. Later in Section 4, we show the accuracy of OPT models quantized using different numbers of row clusters, demonstrating that clustering in addition to partitioning is crucial for improved model accuracy.

4 QUANTIZATION EXPERIMENTS

To study the behavior of quantized LLMs, we apply CVXQ (Algorithm 1) to the quantization of the Meta Open Pretrained Transformer (OPT) (S. Zhang et al., 2022) and Llama-2 (Touvron et al., 2023) families of language models (from the Hugging Face Hub), comparing the performance of CVXQ against other model quantization methods on language modeling and math-word problem solving tasks. For calibration data, we source 100 examples from the training split of the C4 dataset (Raffel et al., 2020) for both tasks and test using the test split of WikiText2 (Merity et al., 2022) for language modeling and the test split of GSM8K (Cobbe et al., 2021) for word math problems. A number of studies on the sensitivity of algorithm hyperparameters are also conducted using the C4 dataset.

Language Modeling. As our main set of experiments, we quantize Meta’s OPT and Llama 2 models to 3 and 4 bits and measure the performance of the quantized models using perplexity, a stringent accuracy metric. We use row clusters with a cluster size of 512 for OPT (768 for OPT-125M) and 256 for Llama 2 models, accumulation batch size of 16, and 17 tokens from each sequence of tokens of length 2048, and optimize for 64 iterations maximum. Table 1 lists the perplexity of our quantized models (CVXQ) on the WikiText2 test set. While we perform quantized model selection based on the WikiText2 validation set, selecting the last quantized model produces similar test accuracy. For comparison, we include the perplexities of the same models quantized with round-to-nearest, GPTQ (Frantar et al., 2022), OWQ (Lee et al., 2024), and AWQ (Lin et al., 2024) methods, using the code provided by the respective authors; see Appendix D for details. Relative to the next best performing methods OWQ and AWQ, the proposed method provides a perplexity reduction of up to 4.55 for the 3-bit OPT-125M model although a minor perplexity gain (0.01–0.02) is observed for 3-bit OPT-66B and Llama 2 70B models. Note that AWQ in this comparison uses a group size of 128, incurring 2–4 times as many overhead bits as the proposed method, and OWQ by its nature operates at average per-weight bit depths that are 0.01–0.05 bits higher than the proposed method.

Effect of Hyperparameters. To study the effect of CVXQ hyperparameters on the accuracy of the quantized models, we quantize the OPT-1.3B and -13B models over a range of minibatch sizes and token counts (optimization hyperparameters) and cluster sizes (quantization hyperparameter), with each hyperparameter varied while keeping the others fixed at their optimized values. (The optimal hyperparameter values are batch size: 16, token count: 17, and cluster size: 512.) The perplexity of the quantized models is then measured on the C4 test data. Table 2 (a–b) demonstrates that CVXQ is largely insensitive to the values of optimization hyperparameters over a wide range. From Table 2 (c), we see that smaller cluster sizes generally improve the performance of the quantized models at lower average bit depths, but this also leads to higher overheads (discussed later). Figure 5 plots quantized model accuracy across optimization iterations when the baseline hyperparameter values are used, showing that about 20 iterations are needed for quantization parameters (clustering and bit

Table 1: WikiText2 perplexity. We quantize the Meta OPT and Llama 2 families of LLMs to 3–4 bits per weight on average using the proposed quantization method, reporting the perplexity of each quantized model on the WikiText2 dataset (test). For comparison, we also include the perplexities of models quantized using other approaches.

| Perplexity (PPL) | | Meta OPT (Open Pretrained Transformer) | | | | | | | Meta Llama 2 | | | |
|-----------------------|-----------------|--|--------------|--------------|--------------|--------------|--------------|-------------|--------------|-------------|-------------|-------------|
| WikiText2 (↓) | | 125M | 350M | 1.3B | 2.7B | 6.7B | 13B | 30B | 66B | 7B | 13B | 70B |
| Full precision (FP16) | | 27.65 | 22.00 | 14.63 | 12.47 | 10.86 | 10.13 | 9.56 | 9.34 | 5.47 | 4.88 | 3.32 |
| 4 bits | RTN | 37.28 | 25.94 | 48.17 | 16.92 | 12.10 | 11.32 | 10.98 | 111.36 | 5.73 | 4.98 | 3.46 |
| | GPTQ | 32.05 | 23.87 | 15.47 | 12.83 | 11.14 | 10.29 | 9.57 | 9.34 | 5.69 | 4.98 | 3.42 |
| | GPTQ/256 | 30.53 | 23.83 | 14.91 | 12.52 | 11.02 | 10.22 | 9.60 | 9.46 | 5.69 | 5.02 | 3.44 |
| | OWQ (4.01 bits) | 29.47 | 23.19 | 15.01 | 12.39 | 10.87 | 10.26 | 9.50 | 9.25 | 5.63 | 5.01 | 3.43 |
| | AWQ | 29.11 | – | 14.95 | 12.74 | 10.93 | 10.22 | 9.59 | 9.39 | 5.60 | 4.97 | 3.41 |
| | CVXQ (Ours) | 27.90 | 22.89 | 14.20 | 12.12 | 10.52 | 10.08 | 9.45 | 9.21 | 5.57 | 4.97 | 3.40 |
| 3 bits | RTN | 1284.92 | 64.57 | 119.47 | 298.00 | 23.54 | 46.04 | 18.80 | 6122.33 | 6.66 | 5.52 | 3.98 |
| | GPTQ | 53.43 | 32.28 | 20.90 | 16.55 | 12.88 | 11.58 | 10.29 | 9.90 | 6.43 | 5.48 | 3.88 |
| | GPTQ/256 | 41.22 | 29.96 | 16.98 | 13.94 | 11.39 | 10.41 | 9.81 | 11.13 | 6.75 | 5.59 | 4.00 |
| | OWQ (3.01 bits) | 35.26 | 26.59 | 16.40 | 13.21 | 11.21 | 11.48 | 9.59 | 9.28 | 6.21 | 5.36 | 3.77 |
| | AWQ | 36.77 | – | 16.32 | 13.54 | 11.41 | 10.67 | 9.85 | 9.63 | 6.24 | 5.32 | 3.74 |
| | CVXQ (Ours) | 30.71 | 25.96 | 14.75 | 12.42 | 11.07 | 10.28 | 9.56 | 9.29 | 6.00 | 5.26 | 3.74 |

Table 2: Effect of hyperparameters on quantized model accuracy. Quantized model accuracy is relatively insensitive to the minibatch size (a) and number of tokens per sequence (b) used for the optimization. Smaller clusters improve quantized model accuracy at low average bit depths (c). All perplexity measured on the C4 test set.

| (a) Minibatch size and PPL | | | | | (b) Number of tokens and PPL | | | | | (c) Cluster size and PPL | | | | | | | |
|----------------------------|--------------|--------------|--------------|--------------|------------------------------|--------------|-----------|--------------|--------------|--------------------------|--------------|--------------|--------------|--------------|--------------|--------------|--------------|
| PPL | OPT (4 bits) | | OPT (3 bits) | | PPL | OPT (4 bits) | | OPT (3 bits) | | PPL | OPT (4 bits) | | OPT (3 bits) | | | | |
| C4 (↓) | 1.3B | 13B | 1.3B | 13B | C4 (↓) | 1.3B | 13B | 1.3B | 13B | C4 (↓) | 1.3B | 13B | 1.3B | 13B | | | |
| FP16 | 16.07 | 12.06 | 16.07 | 12.06 | FP16 | 16.07 | 12.06 | 16.07 | 12.06 | FP16 | 16.07 | 12.06 | 16.07 | 12.06 | | | |
| Batch size | 2 | 16.24 | 12.12 | 16.94 | 12.36 | Num tokens | 3 | 16.40 | 12.29 | 17.05 | 12.47 | Cluster size | 64 | 16.16 | 12.10 | 16.62 | 12.26 |
| | 4 | 16.24 | 12.12 | 16.94 | 12.35 | | 5 | 16.28 | 12.18 | 16.93 | 12.37 | | 128 | 16.17 | 12.10 | 16.70 | 12.29 |
| | 8 | 16.25 | 12.11 | 16.90 | 12.34 | | 9 | 16.24 | 12.12 | 16.91 | 12.35 | | 256 | 16.20 | 12.10 | 16.77 | 12.32 |
| | 16 | 16.22 | 12.11 | 16.86 | 12.32 | | 17 | 16.22 | 12.11 | 16.86 | 12.32 | | 512 | 16.22 | 12.11 | 16.86 | 12.32 |
| | 32 | 16.24 | 12.12 | 16.88 | 12.36 | | 33 | 16.21 | 12.10 | 16.87 | 12.34 | | 1024 | 16.23 | 12.11 | 16.99 | 12.42 |

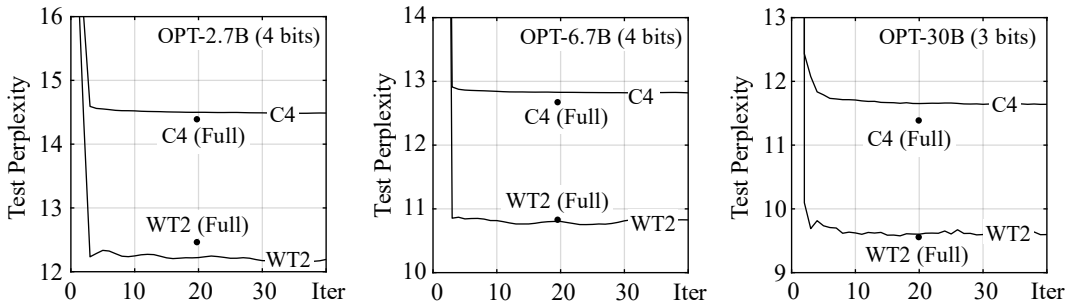


Figure 5: Test perplexity across iterations. Calibrated on C4 (train) using a batch size of 16. Row clusters of size 512 used. Perplexity decreases rapidly within the first 30 iterations, monotonically for C4 (test), whose distribution is similar to the calibration data, and with some oscillations in the case of WikiText2 (test), whose distribution is less similar.

depth decisions) to reach their optimal values.

Pruning Due to Quantization. CVXQ quantizes low-variance weights of weight matrices to zero and effects a form of weight pruning, which has been shown to improve generalization (Hassibi & Stork, 1992). Table 3 (a) lists the percentages of zero-quantized weights in the OPT-1.3B and 13B models quantized to 3 and 4 bits per weight on average. We observe that using smaller cluster sizes increases the number of pruned weights since this enables low-variance weights in each column to be clustered together and quantized to zero. However, smaller clusters lead to higher overheads so that small improvements in generalization due to pruning come at the cost of signaling the overhead bits. Table 3 (b) lists the number of overhead bits (cluster indices and FP16 encodings of the location

Table 3: Pruning and overhead bits. A small fraction of weights is quantized to zero and pruned away due to low variance, with smaller clusters increasing the degree of pruning (a). Quantization incurs overhead bits for signaling cluster indices and location and scale parameters of each weight cluster (b).

| (a) Pruned columns (%) in quantized models | | | | | | | (b) Overhead bits (%) from quantization parameters | | | | | | | |
|--|--------------|-------------|-------------|--------------|-------------|-------------|--|--------------|-------------|-------------|--------------|-------------|-------------|-------------|
| Pruned (%) | OPT (4 bits) | | | OPT (3 bits) | | | Overhead bits (%) | OPT (4 bits) | | | OPT (3 bits) | | | |
| | 350M | 1.3B | 13B | 350M | 1.3B | 13B | | 350M | 1.3B | 13B | 350M | 1.3B | 13B | 30B |
| Cluster size 64 | 0.57 | 2.13 | 2.18 | 0.64 | 3.70 | 3.12 | 64 | 10.33 | 10.30 | 10.28 | 13.77 | 13.73 | 13.71 | 13.70 |
| 128 | 0.61 | 2.19 | 2.31 | 0.68 | 3.81 | 3.04 | 128 | 5.18 | 5.16 | 5.15 | 6.91 | 6.88 | 6.87 | 6.86 |
| 256 | 0.67 | 2.10 | 2.16 | 0.69 | 3.06 | 2.69 | 256 | 2.60 | 2.59 | 2.58 | 3.47 | 3.45 | 3.44 | 3.44 |
| 512 | 0.68 | 2.07 | 2.00 | 0.70 | 2.85 | 2.57 | 512 | 1.30 | 1.30 | 1.30 | 1.73 | 1.73 | 1.73 | 1.72 |
| 1024 | 0.68 | 2.08 | 1.92 | 0.70 | 2.39 | 2.26 | 1024 | 0.64 | 0.65 | 0.65 | 0.85 | 0.87 | 0.87 | 0.86 |

Table 4: Grade School Math 8K (GSM8K) and 2.x-bit quantization. Quantized model accuracy measured by performance on tasks such as GSM8K (a). Cluster size of 256 is used). Quantized to 2.x bits per weight on average, CVXQ reduces perplexity considerably when compared with OWQ models quantized to the same (b).

| (a) Percentage score of correct answers on GSM8K | | | | | | | (b) Perplexity of 2.1–2.8 bit-quantized models | | | | | | |
|--|------------------|--------------|--------------|------------------|--------------|--------------|--|---------------------------|---------------|-------------|-------------|-------------|-------|
| Score (%) | Llama 2 (4 bits) | | | Llama 2 (3 bits) | | | Perplexity | Llama 2 7B (2.1–2.8 bits) | | | | | |
| | GSM8K (↑) | 7B | 13B | 70B | 7B | 13B | | 70B | WikiText2 (↓) | 2.1 | 2.2 | 2.4 | 2.6 |
| FP16 | 14.10 | 23.43 | 53.90 | 14.10 | 23.43 | 53.90 | FP16 | 5.47 | 5.47 | 5.47 | 5.47 | 5.47 | 5.47 |
| RTN | 7.05 | 19.11 | 46.93 | 1.82 | 1.67 | 6.14 | OWQ | 39.56 | 11.25 | 10.79 | 10.43 | 10.24 | 10.24 |
| GPTQ/256 | 11.60 | 21.46 | 52.01 | 6.60 | 14.48 | 46.47 | OWQ/256 | 10.34 | 10.01 | 9.98 | 9.50 | 9.26 | |
| AWQ/256 | 14.33 | 23.12 | 50.34 | 6.97 | 16.76 | 48.07 | OWQ/128 | 10.01 | 9.66 | 9.42 | 9.38 | 9.14 | |
| CVXQ/256 | 12.74 | 23.05 | 53.37 | 8.87 | 18.04 | 48.60 | CVXQ/256 | 9.47 | 8.39 | 7.05 | 6.56 | 6.21 | |

and scale parameters of each weight cluster) as a percentage of the total quantized weight bits. These overheads are in line with those of other algorithms which must similarly signal zero points and step sizes of the quantization grid (Lee et al., 2024).

Downstream Tasks (Grade School Math 8K). To study the impact of quantization on downstream tasks, we list in Table 4 (a) the accuracy of CVXQ-quantized Llama-2 models on the GSM8K (Grade School Math 8K) task (Cobbe et al., 2021), designed to evaluate the ability of language models to solve grade-level math word problems. Evaluation is performed in a 5-shot setup (flexible-extract filter). We set our cluster size and the group size of GPTQ and AWQ to 256. We observe that CVXQ produces slightly higher scores than the GPTQ and AWQ quantized 3-bit models while RTN leads to severely diminished scores despite having similar perplexity scores as CVXQ on WikiText2; see Table 1. We include examples of output from different quantized models in Appendix E.

2.x-bit Llama-2. We study the accuracy of Llama 2 models quantized to 2.x bits using CVXQ and OWQ, both of which are capable of quantizing models to fractional average bit depths. To enable a more comprehensive study, we compare against OWQ with no grouping, as well as with group sizes of 128 and 256. We see from Table 4 (b) that CVXQ-quantized Llama-2 models are considerably more accurate at these bit depths than their OWQ counterparts. This is expected since CVXQ assigns bit depths from the range $(0, B_{\max})$ commensurately with gradient variances whereas OWQ opts to preserve the most sensitive (highest-variance) weights in FP16 and quantize the rest to 2 bits (Lee et al., 2024). In terms of execution time, CVXQ (64 iterations) and OWQ/GPTQ require 47 minutes and 18 minutes, respectively (excluding validation), to quantize the 7B model on an Nvidia A100.

5 DISCUSSION

Formulating weight quantization as a convex optimization problem, as we have done here, bestows several benefits. First, it explicates the objective we seek to optimize (minimizing output distortion in our case) and sets us on a path to solve the right problem using modern automatic differentiation tools e.g. PyTorch’s autograd package. Second, our formulation enables us to interpret many earlier Hessian-based methods (Frantar et al., 2022; Lee et al., 2024; Dong et al., 2019; Chen et al., 2021) as heuristics for approximate optimization of the true underlying quantization objective. Note that (2) is a nonlinear system of equations in the bit depth variables, so that any non-iterative solution is

necessarily only an approximate one if one’s goal is to optimize an objective similar to (2). Recent high-performing model quantization methods (Frantar et al., 2022; Frantar & Alistarh, 2022; Lee et al., 2024) ultimately trace their lineage back to the classic Optimal Brain Surgeon algorithm (Hassibi & Stork, 1992), which is a convex formulation of weight pruning, as opposed to quantization (see Appendix C). As a result, these methods inherit the need for fine-tuning as part of the quantization process, making them less suitable for the quantization of activations during inference, where fine-tuning of activations would lead to unacceptable delays in the inference pipeline.

Our experimental results indicate that an accurate characterization of the quantization problem can indeed lead to better compression outcomes. While the smaller OPT-125M model is too limited for practical use in many situations, its relative incompressibility helps contrast the performance of the different weight quantization methods themselves (Table 1). With larger models like OPT-66B and Llama 2-66B, most approaches (including RTN) perform similarly, suggesting that larger language models are more compressible in general. At first glance, RTN may seem sufficient for quantizing larger models. However, RTN-quantized models lead to severely reduced accuracy on downstream tasks such as GSM8K (Table 4 (a)), which highlights the importance of validating the accuracy of quantized models across multiple tasks and datasets. Increasing the number of calibration examples (from 100 to 1000) does not appear to noticeably affect the quantized model’s performance, which agrees with findings from previous reports (Hubara et al., 2021).

Limitations and future work. The end-to-end nature of our optimization algorithm can also be its own weakness, as convergence can be slower for lower-bit (2 bit) instances of problem (3) and the algorithm can require more hardware resources than previous approaches. Extension work currently underway for weight quantization includes faster optimizers and efficient compander design. Unlike GPTQ and its extensions, in which each linear layer is essentially retrained during quantization, the proposed method spends most of its running time on the collection of channel statistics (squares of gradients) and very little time on the actual quantization process. This allows us to apply CVXQ also to activation quantization, where quantization efficiency becomes paramount. We discuss activation quantization and CUDA implementation of joint weight and activation quantization in Part 2.

REPRODUCIBILITY

To ensure the reproducibility of results in this work, we make our PyTorch CVXQ code available on our GitHub project website, where readers can also ask questions about this work. Appendices A–B provide derivations for our main theoretical results. Appendix D additionally details the code and command line options used to obtain the results of GPTQ (Frantar et al., 2022), OWQ (Lee et al., 2024), and AWQ (Lin et al., 2024).

REFERENCES

- Stephen Boyd, Neal Parikh, Eric Chu, Borja Peleato, and Jonathan Eckstein. Distributed optimization and statistical learning via the alternating direction method of multipliers. *Found. Trends® Mach. Learn.*, 3(1):1–122, 2011.
- Weihan Chen, Peisong Wang, and Jian Cheng. Towards mixed-precision quantization of neural networks via constrained optimization. In *Proc ICCV*, 2021.
- Kanghyun Choi, Deokki Hong, Noseong Park, Youngsok Kim, and Jinho Lee. Qimera: Data-free quantization with synthetic boundary supporting samples. In *Proc. NeurIPS*, 2021.
- Yoojin Choi, Mostafa El-Khamy, and Jungwon Lee. Towards the limits of network quantization. In *Proc. ICLR*, 2017.
- Karl Cobbe, Vineet Kosaraju, Mohammad Bavarian et al. Training verifiers to solve math word problems. <http://arxiv.org/abs/2110.14168>, 2021.
- Thomas M. Cover, and Joy A. Thomas. Elements of Information Theory (Wiley Series in Telecommunications and Signal Processing). Wiley-Interscience, USA 2006.
- Tim Dettmers, Mike Lewis, Younes Belkada, and Luke Zettlemoyer. GPT3.int8(): 8-bit matrix multiplication for transformers at scale. In *Proc. NeurIPS*, 2022.

- Tim Dettmers, Ruslan Svirschevski, Vage Egiazarian et al. SpQR: A Sparse-Quantized Representation for near-lossless LLM weight compression. <http://arxiv.org/abs/2306.03078>, 2023.
- Zhen Dong, Zhewei Yao, Amir Gholami, Michael W. Mahoney, and Kurt Keutzer. HAWQ: Hessian AWare Quantization of neural networks with mixed precision. In *Proc. ICCV*, 2019.
- Vage Egiazarian, Andrei Panferov, Denis Kuznedev, Elias Frantar, Artem Babenko, and Dan Alistarh. Extreme compression of large language models via additive quantization. In *Proc. ICML*, 2024.
- Steven K. Esser, Jeffrey L. McKinstry, Deepika Bablani, Rathinakumar Appuswamy, and Dharmendra S. Modha. Learned step size quantization. In *Proc. ICLR*, 2019.
- Elias Frantar, and Dan Alistarh. Optimal Brain Compression: A framework for accurate post-training quantization and pruning. In *Proc. NeurIPS*, 2022.
- Elias Frantar, Saleh Ashkboos, Torsten Hoefler, and Dan Alistarh. OPTQ: Accurate quantization for generative pre-trained transformers. In *Proc. ICLR*, 2022.
- Allen Gersho, and Robert M. Gray. Vector Quantization and Signal Compression. Kluwer, Norwell, MA, USA 1991.
- Yunchao Gong, Liu Liu, Ming Yang, and Lubomir Bourdev. Compressing deep convolutional networks using vector quantization. In *Proc. ICLR*, 2015.
- R.M. Gray, and D.L. Neuhoff. Quantization. *IEEE Trans. Inf. Theory*, 44(6):2325–2383, 1998.
- Ziyi Guan, Hantao Huang, Yupeng Su, Hong Huang, Ngai Wong, and Hao Yu. APTQ: Attention-aware post-training mixed-precision quantization for large language models. In *Proc. DAC*, 2024.
- Babak Hassibi, and David Stork. Second order derivatives for network pruning: Optimal Brain Surgeon. In *Proc. NIPS*, 1992.
- Lu Hou, and James T. Kwok. Loss-aware weight quantization of deep networks. In *Proc. ICLR*, 2018.
- Wei Huang, Haotong Qin, Yangdong Liu et al. Slim-LLM: Saliency-driven mixed-precision quantization for large language models, <https://arxiv.org/abs/2405.14917v1>, 2024.
- Itay Hubara, Yury Nahshan, Yair Hanani, Ron Banner, and Daniel Soudry. Accurate post training quantization with small calibration sets. In *Proc. ICML*, 2021.
- Benoit Jacob, Skirmantas Kligys, Bo Chen et al. Quantization and training of neural networks for efficient integer-arithmetic-only inference. In *Proc. CVPR*, 2018.
- Sehoon Kim et al. SqueezeLLM: Dense-and-sparse quantization. In *Proc. ICML*, 2024.
- Changhun Lee, Jungyu Jin, Taesu Kim, Hyungjun Kim, and Eunhyeok Park. OWQ: Outlier-aware weight quantization for efficient fine-tuning and inference of large language models. In *Proc. AAAI*, 2024.
- Ji Lin, Jiaming Tang, Haotian Tang et al. AWQ: Activation-aware Weight Quantization for on-device LLM compression and acceleration. In *Proc. MLSys*, 2024.
- S. Lloyd. Least squares quantization in PCM. *IEEE Trans. Inf. Theory*, 28(2):129–137, 1982.
- J. Max. Quantizing for minimum distortion. *IRE Trans. Inf. Theory*, 6(1):7–12, 1960.
- Stephen Merity, Caiming Xiong, James Bradbury, and Richard Socher. Pointer sentinel mixture models. In *Proc. ICLR*, 2022.
- Markus Nagel, Mart van Baalen, Tijmen Blankevoort, and Max Welling. Data-free quantization through weight equalization and bias correction. In *Proc. CVPR*, 2019.
- Yury Nahshan, Brian Chmiel, Chaim Baskin, Evgenii Zheltonozhskii, Ron Banner, Alex M. Bronstein, and Avi Mendelson. Loss aware post-training quantization. In *Mach Learn* 110 3245–3262, Springer, 2020.
- Jorge Nocedal, and Stephen J. Wright. Numerical Optimization. Springer, New York, NY, USA 2009.

- Biao Qian, Yang Wang, Richang Hong, and Meng Wang. Adaptive data-free quantization. In *Proc. CVPR*, 2023.
- Zhongnan Qu, Zimu Zhou, Yun Cheng, and Lothar Thiele. Adaptive loss-aware quantization for multi-bit networks. In *Proc. CVPR*, 2020.
- Colin Raffel, Noam Shazeer, Adam Roberts et al. Exploring the limits of transfer learning with a unified text-to-text transformer. *J. Mach. Learn. Res.*, 21(140):1–67, 2020.
- Wenqi Shao et al. OmniQuant: Omnidirectionally calibrated quantization for large language models. In *Proc. ICLR*, 2024.
- Hugo Touvron, Louis Martin, Kevin Stone et al. Llama 2: Open foundation and fine-tuned chat models. <http://arxiv.org/abs/2307.09288>, 2023.
- Vincent Vanhoucke, Andrew Senior, and Mark Z. Mao. Improving the speed of neural networks on CPUs. In *Proc. NIPS Workshops*, 2011.
- Kuan Wang, Zhijian Liu, Yujun Lin, Ji Lin, and Song Han. HAQ: Hardware-aware automated quantization with mixed precision. In *Proc. CVPR*, 2019.
- Guangxuan Xiao, Ji Lin, Mickael Seznec, Hao Wu, Julien Demouth, and Song Han. SmoothQuant: Accurate and efficient post-training quantization for large language models. In *Proc. ICML*, 2023.
- Shoukai Xu, Haokun Li, Bohan Zhuang, Jing Liu, Jiezhong Cao, Chuangrun Liang, and Mingkui Tan. Generative low-bitwidth data free quantization. In *Proc. ECCV*, 2020.
- Zhewei Yao, Reza Yazdani Aminabadi, Minjia Zhang, Xiaoxia Wu, Conglong Li, and Yuxiong He. ZeroQuant: Efficient and affordable post-training quantization for large-scale transformers. In *Proc. NeurIPS*, 2022.
- Sean I. Young, Wang Zhe, David Taubman, and Bernd Girod. Transform quantization for CNN compression. *IEEE Trans. Pattern Anal. Mach. Intell.*, 44(9):5700–5714, 2019.
- Zhihang Yuan, Yuzhang Shang, Yang Zhou et al. LLM inference unveiled: Survey and roofline model insights. <https://arxiv.org/abs/2402.16363>, 2024.
- Dongqing Zhang, Jiaolong Yang, Dongqiangzi Ye, and Gang Hua. LQ-Nets: Learned quantization for highly accurate and compact deep neural networks. In *Proc. ECCV*, 2018.
- Susan Zhang, Stephen Roller, Naman Goyal et al. OPT: Open Pre-trained Transformer Language Models. <http://arxiv.org/abs/2205.01068>, 2022.
- Ritchie Zhao, Yuwei Hu, Jordan Dotzel, Chris De Sa, and Zhiru Zhang. Improving neural network quantization without retraining using outlier channel splitting. In *Proc. ICML*, 2019.
- Aojun Zhou, Anbang Yao, Yiwen Guo, Lin Xu, and Yurong Chen. Incremental Network Quantization: towards lossless CNNs with low-precision weights. In *Proc. ICLR*, 2017.

A DERIVATION OF EQUATION (5)

To derive our main equation (5), we appeal to a linearized relationship between model weights and output, as well as standard results from rate–distortion theory (Gersho & Gray, 1991) that relate the quantization error of a random source to output distortion at a high bit depth, where the linearized model relationship is a good approximation. Let us start with our quantization objective

$$d(B_1, B_2, \dots, B_N) = \mathbb{E}_{\mathbf{X}} \|f(\mathbf{X}, \Theta_1^q(B_1), \Theta_2^q(B_2), \dots, \Theta_N^q(B_N)) - f(\mathbf{X})\|_F^2, \quad (10)$$

in which $f(\mathbf{X}) = f(\mathbf{X}, \Theta_1(B_1), \Theta_2(B_2), \dots, \Theta_N(B_N))$ denotes the output of the unquantized model given input \mathbf{X} . We can write the residual and Jacobian of f at $(\mathbf{X}, \Theta_1^q(B_1), \Theta_2^q(B_2), \dots, \Theta_N^q(B_N))$ as

$$r(\mathbf{X}, \Theta_1^q, \Theta_2^q, \dots, \Theta_N^q) = (r_1, \dots, r_M)(\mathbf{X}, \Theta_1^q, \Theta_2^q, \dots, \Theta_N^q) = f(\mathbf{X}, \Theta_1^q, \Theta_2^q, \dots, \Theta_N^q) - f(\mathbf{X})$$

$$J(\mathbf{X}, \Theta_1^q, \Theta_2^q, \dots, \Theta_N^q) = \left(\frac{\partial f(\mathbf{X}, \Theta_1^q, \dots, \Theta_N^q)}{\partial \Theta_1}, \frac{\partial f(\mathbf{X}, \Theta_1^q, \dots, \Theta_N^q)}{\partial \Theta_2}, \dots, \frac{\partial f(\mathbf{X}, \Theta_1^q, \dots, \Theta_N^q)}{\partial \Theta_N} \right) \quad (11)$$

and proceed to write the gradient and Hessian of the objective (10) in terms of the r and J above as

$$\begin{aligned}\nabla d(\mathbf{X}, \boldsymbol{\Theta}_1^q, \boldsymbol{\Theta}_2^q, \dots, \boldsymbol{\Theta}_N^q) &= (J^T r)(\mathbf{X}, \boldsymbol{\Theta}_1^q, \boldsymbol{\Theta}_2^q, \dots, \boldsymbol{\Theta}_N^q) \\ \nabla^2 d(\mathbf{X}, \boldsymbol{\Theta}_1^q, \boldsymbol{\Theta}_2^q, \dots, \boldsymbol{\Theta}_N^q) &= (J^T J)(\mathbf{X}, \boldsymbol{\Theta}_1^q, \boldsymbol{\Theta}_2^q, \dots, \boldsymbol{\Theta}_N^q) + \underbrace{\sum_{m=1}^M (r_m \nabla^2 r_m)(\mathbf{X}, \boldsymbol{\Theta}_1^q, \boldsymbol{\Theta}_2^q, \dots, \boldsymbol{\Theta}_N^q)}_{\approx 0}\end{aligned}\quad (12)$$

in which the second term of $\nabla^2 f$ is approximately zero either because the residuals r_m are relatively small, or they are close to affine in $(\Delta_1^q, \Delta_2^q, \dots, \Delta_N^q)$ so that $\nabla^2 r_m$ are relatively small, which is the case in the vicinity of the solution.

Using (12), we can now express the local quadratic approximation of (10) about (B_1, \dots, B_N) as

$$\begin{aligned}\hat{d}(B_1, \dots, B_N) &\stackrel{(a)}{=} \mathbb{E}_{\mathbf{X}} \left[(\Delta_1^q(B_1), \dots, \Delta_N^q(B_N)) \left((J^T J)(\mathbf{X}, \boldsymbol{\Theta}_1^q, \dots, \boldsymbol{\Theta}_N^q) \right) (\Delta_1^q(B_1), \dots, \Delta_N^q(B_N))^T \right] \\ &\quad + \underbrace{\mathbb{E}_{\mathbf{X}} \left[(\Delta_1(B_1), \dots, \Delta_N(B_N))^T \left((J^T r)(\mathbf{X}, \boldsymbol{\Theta}_1^q, \boldsymbol{\Theta}_2^q, \dots, \boldsymbol{\Theta}_N^q) \right) \right]}_{=0} \\ &\stackrel{(b)}{=} \sum_{n=1}^N \mathbb{E}_{\mathbf{X}} [(J^T J)_{nn}(\mathbf{X}, \boldsymbol{\Theta}_1^q, \dots, \boldsymbol{\Theta}_N^q)] \mathbb{E}[\Delta_n^2(B_n)] \stackrel{(c)}{=} \sum_{n=1}^N \underbrace{P_n G_n^2 H_n S_n^2 2^{-2B_n}}_{=d_n(B_n)}\end{aligned}\quad (13)$$

in which the zero expectation of the linear term in (a) follows from the zero means of quantization errors $\Delta_1, \dots, \Delta_N$, (b) follows from the uncorrelatedness of $\Delta_1, \dots, \Delta_N$, and (c) follows from our definition of gradient variance $G_n^2 = P_n^{-1} \mathbb{E}_{\mathbf{X}} [(J^T J)_{nn}(\mathbf{X}, \boldsymbol{\Theta}_1^q, \dots, \boldsymbol{\Theta}_N^q)]$ together with the result from rate–distortion theory (Gersho & Gray, 1991) that relates the variance of random quantization error $\mathbb{E}[\Delta_n^2(B_n)] = H_n S_n^2 2^{-2B_n}$ to the variance S_n^2 of the random source, and the coefficient H_n , and bit depth B_n of quantization. Expression (5) for the partial derivatives of d with respect to B_n follows directly from the properties of the derivative of an exponential.

Since (10) is a non-linear least-squares objective and its gradient depends on the gradient variances $G_1^2, G_2^2, \dots, G_N^2$, its minimization requires an iterative update of $\boldsymbol{\Theta}_1^q, \boldsymbol{\Theta}_2^q, \dots, \boldsymbol{\Theta}_N^q$ via the choice of B_1, B_2, \dots, B_N and re-evaluation of the gradient variances $G_1^2, G_2^2, \dots, G_N^2$ at $\boldsymbol{\Theta}_1^q, \boldsymbol{\Theta}_2^q, \dots, \boldsymbol{\Theta}_N^q$. This is similar to the local Hessian evaluated by the Gauss–Newton method (Nocedal & Wright, 2006) every time the descent direction is re-computed. One can think of $G_1^2, G_2^2, \dots, G_N^2$ as the diagonal elements of a non-diagonal Hessian matrix used in e.g. the Gauss–Newton method, but whose off-diagonal elements disappear in the expectation due to multiplication by uncorrelated quantization errors $\Delta_1^q, \dots, \Delta_N^q$.

B DERIVATION OF EQUATION (8)

To derive our sigmoid companding function (8), we turn to results from rate–distortion theory that relate the mean square error of quantization of weights θ to the density p_θ of θ and the density $\lambda(\theta)$ of quantization levels, where $2^B \int_a^b \lambda(\theta) d\theta$ expresses the number of quantization levels of a B -bit quantizer within any interval $[a, b]$. Writing Π_i for the i th quantization cell and $\Pi(\theta)$ for the width of the cell containing θ , we can write the mean square error of quantized weights as

$$\begin{aligned}\mathbb{E}|\theta - \theta^q|^2 &= \sum_{i=1}^{2^B} \mathbb{P}[\theta \in \Pi_i] \mathbb{E}[|\theta - \theta^q|^2 | \theta \in \Pi_i] \\ &\stackrel{(a)}{\approx} \sum_{i=1}^{2^B} \mathbb{P}[\theta \in \Pi_i] \frac{|\Pi_i|^2}{12} \stackrel{(b)}{\approx} \int p_\theta(\theta) \frac{\Pi^2(\theta)}{12} d\theta \\ &\stackrel{(c)}{\approx} \frac{1}{2^{2B}} \int p_\theta(\theta) \frac{\lambda^{-2}(\theta)}{12} d\theta\end{aligned}\quad (14)$$

in which (a) follows from our assumption that weight distribution is approximately uniform within each quantization cell, (b) follows from an integral approximation of the finite sum, and (c) follows from the relationship $2^B \lambda^{-1}(\theta) = \Pi(\theta)$, all of which hold approximately when B is sufficiently large.

To find the density λ of quantization levels that leads to the minimum quantization error when θ has density p_θ , we use Hölder's inequality: $\int p_\theta^{1/3} \leq (\int p_\theta \lambda^{-2})^{1/3} (\int \lambda)^{2/3}$. Since $\int \lambda = 1$, we have that $\int p_\theta \lambda^{-2} \geq (\int p_\theta^{1/3})^3$, which sets a lower bound on the last term of (14). This lower bound and hence minimum quantization error is attained iff $p_\theta \lambda^{-2} \propto \lambda$. The optimal density for quantization levels is therefore given by

$$\lambda(\theta) \propto p_\theta^{1/3}(\theta) \Leftrightarrow \Pi^{-1}(\theta) \propto p_\theta^{1/3}(\theta). \quad (15)$$

Rather than optimize the density λ to minimize the quantization error for a given p_θ , we could equivalently transform the weights θ as $\theta^\sigma = \sigma(\theta)$ via a non-linear σ , so that uniform quantization applied to $\theta^\sigma \sim p_{\theta^\sigma}$ leads to the same minimum quantization error. The width $\Pi(\theta)$ of non-uniform quantization cells quantizing θ relate to the width of uniform quantization cells of the companded (transformed) weights $\theta^\sigma = \sigma(\theta)$ as

$$d\sigma(\theta) = \frac{d\theta}{\Pi(\theta)} \propto p_\theta^{1/3}(\theta) d\theta \Rightarrow \sigma'(\theta) \propto p_\theta^{1/3}(\theta), \quad (16)$$

in which the first proportionality follows from (15). We can find the optimal nonlinear transform σ by integrating $p_\theta^{1/3}(\theta)$ and normalizing (for convenience) the range of the integral to $[0, 1]$:

$$\sigma(\theta) = \left(\int_{-\infty}^{\theta} p_\theta^{1/3}(t) dt \right)^{-1} \left(\int_{-\infty}^{\theta} p_\theta^{1/3}(t) dt \right) \quad (17)$$

(Gersho & Gray, 1991). Finally, we obtain (8) by substituting the expression for the density of a Laplace distribution (parameterized by mean μ and standard deviation S) into p_θ above. Transform σ is asymptotically optimal as $B \rightarrow \infty$ in (14).

C CONVEX WEIGHT PRUNING (HASSABI & STORK, 1992)

To facilitate comparison between convex weight quantization (this work) and the convex weight pruning work of Hassabi & Stork (1992), we provide a derivation of Hassabi & Stork's Optimum Brain Surgeon (OBS) algorithm (presented slightly differently), together with our commentary for additional clarification.

For simplicity, let us rewrite model (4) as $f(\cdot, \Theta_1, \Theta_2, \dots, \Theta_N) = f(\cdot, \Theta)$, where Θ is a vector of all model weights across different layers of the model. The objective of convex weight pruning is to set some number of elements of Θ to zero while fine-tuning the remaining elements to minimize the difference between the output of the pruned model $f(\cdot, \Theta^p)$ and the output of the unpruned model $f(\cdot, \Theta)$. Writing the pruned weights as $\Theta^p = \Theta + \Delta^p$, where Δ^p is a vector of updates to be made to weights Θ , it is apparent that $\Delta_i^p = -\theta_i$ if the i th weight is to be pruned, otherwise Δ_i^p should be chosen to maximally compensate for the effect of other pruned weights on the output. Suppose we have decided to prune the p th element of Θ . The updated set of weights Θ^p can be found by solving

$$\begin{aligned} \text{minimize } d(\Delta^p) &= \mathbb{E}_{\mathbf{X}} \|f(\mathbf{X}, \Theta + \Delta^p) - f(\mathbf{X}, \Theta)\|_2^2 \approx \mathbb{E}_{\mathbf{X}} [\Delta^{pT} (J^T J)(\mathbf{X}, \Theta) \Delta^p] \\ \text{subject to } r(\Delta^p) &= \mathbf{e}_p^T \Delta^p - \theta_p = 0 \end{aligned} \quad (18)$$

in which $J(\mathbf{X}, \Theta)$ represents the Jacobian of $f(\mathbf{X}, \Theta)$ with respect to Θ , and \mathbf{e}_p^T is an operator that picks out the p th element of a vector. The Lagrangian of this problem becomes

$$\mathcal{L}(\Delta^p, \lambda) = \frac{1}{2} \mathbb{E}_{\mathbf{X}} [\Delta^{pT} (J^T J)(\mathbf{X}, \Theta) \Delta^p] + \lambda (\mathbf{e}_p^T \Delta^p - \theta_p) \quad (19)$$

in which λ represents the dual variable associated with the equality constraint $\mathbf{e}_p^T \Delta^p - \theta_p = 0$.

To solve (18), we differentiate \mathcal{L} with respect to Δ^p , λ and set all obtained derivatives equal to 0 to obtain the first-order optimality conditions $\mathbb{E}_{\mathbf{X}} [(J^T J)(\mathbf{X}, \Theta)] \Delta^p + \mathbf{e}_p \lambda = \mathbf{0}$ and $\mathbf{e}_p^T \Delta^p - \theta_p = 0$. After some algebraic manipulations, we obtain the optimizing values

$$\Delta^p = -\mathbb{E}_{\mathbf{X}} [(J^T J)(\mathbf{X}, \Theta)]^{-1} \mathbf{e}_p \lambda, \quad \lambda = -\frac{\theta_p}{\mathbb{E}_{\mathbf{X}} [(J^T J)(\mathbf{X}, \Theta)]_{pp}^{-1}}, \quad (20)$$

in which the expression for λ is obtained by substituting the expression for Δ^p above into the second optimality condition $\mathbf{e}_p^T \Delta^p - \theta_p = 0$ and solving for λ . Combining both expressions finally produces an update Δ^p that minimizes the objective in (18):

$$\Delta^p = -\frac{\theta_p}{\mathbb{E}_{\mathbf{X}}[(J^T J)(\mathbf{X}, \Theta)]_{pp}^{-1}} \mathbb{E}_{\mathbf{X}}[(J^T J)(\mathbf{X}, \Theta)]^{-1} \mathbf{e}_p, \quad d(\Delta^p) = \frac{1}{2} \frac{\theta_p^2}{\mathbb{E}_{\mathbf{X}}[(J^T J)(\mathbf{X}, \Theta)]_{pp}^{-1}}. \quad (21)$$

So far, we assumed that we were given the index p of the weight to prune from Θ . To actually pick the best weights to prune away, we can compute the pruning loss $d(\Delta^i)$ for all indices i , picking the index i associated with minimum loss. That is,

$$p = \operatorname{argmin}_i \frac{1}{2} \frac{\theta_i^2}{\mathbb{E}_{\mathbf{X}}[(J^T J)(\mathbf{X}, \Theta)]_{ii}^{-1}}, \quad (22)$$

after which Δ^p can be calculated (and consequently Θ^p), and further weights to prune can be picked by initializing $\Theta \leftarrow \Theta^p$ and repeating the process until some pruning criterion has been met.

D ALGORITHM PARAMETERS

To aid the reproducibility of the results in Table 1, we document the code we used for all algorithms (RTN, GPTQ, OWQ, and AWQ) along with the command line arguments.

RTN. We use the OWQ code from <https://github.com/xvyaward/owq/tree/03cfc99> in the provided `owq` conda environment. In the case of e.g. Llama-2-7b-hf quantized to 3 bits, we run `python main.py meta-llama/Llama-2-7b-hf c4 --wbits 3 --nearest`.

GPTQ. We use the OWQ code from <https://github.com/xvyaward/owq/tree/03cfc99> in the provided `owq` conda environment. In the case of e.g. Llama-2-7b-hf quantized to 3 bits, we run the provided command `python main.py meta-llama/Llama-2-7b-hf c4 --wbits 3`. For results based on the group size of 256, we run `python main.py meta-llama/Llama-2-7b-hf c4 --wbits 3 -groupsize 256`.

OWQ. We use the OWQ code from <https://github.com/xvyaward/owq/tree/03cfc99> in the provided `owq` conda environment. In the case of e.g. Llama-2-7b-hf quantized to 3.01 bits, we run the provided command `python main.py meta-llama/Llama-7b-hf c4 --wbits 3 --target_bit 3.01`.

AWQ. We use the AWQ code <https://github.com/mit-han-lab/llm-awq/tree/3665e1a> in the provided `awq` conda environment. In the case of e.g. Llama-2-7b-hf quantized to 3 bits, we run the provided command `python -m awq.entry -model_path meta-llama/Llama-7b-hf --w_bit 3 --q_group_size 128 --run_awq --tasks wikitext`.

E OUTPUT PRODUCED BY DIFFERENT QUANTIZED MODELS

Table 5 lists output produced by different quantized Llama-2-70b models in response to questions taken from the GSM8K dataset. For each question, a prompt is created by prepending the question text with five other question and target pairs from the dataset (known as a 5-shot evaluation). This allows the model to establish a context for the required output and format. It is interesting to note that severe quantization errors (as in the case of RTN) manifest as non sequiturs and errors in logic rather than unintelligible output.

Table 5: Output to questions from the GSM8K dataset (test). Scores shown parentheses are computed across 1319 answers obtained using the flexible extract filter.

| Question | Target | FP16 (Score: 53.90%) | RTN (Score: 6.14%) | GPTQ (Score: 46.47%) | CVXQ (Score: 48.60%) |
|---|---|---|---|--|---|
| Question: Every day, Wendi feeds each of her chickens three cups of mixed chicken feed, containing seeds, mealworms and vegetables to help keep them healthy. She gives the chickens their feed in three separate meals. In the morning, she gives her flock of chickens 15 cups of feed. In the afternoon, she gives her chickens another 25 cups of feed. How many cups of feed does she need to give her chickens in the final meal of the day if the size of Wendi's flock is 20 chickens? Answer: | If each chicken eats 3 cups of feed per day, then for 20 chickens they would need $3 \times 20 = 60$ cups of feed per day. If she feeds the flock 15 cups of feed in the morning, and 25 cups in the afternoon, then the final meal would require $60 - 15 - 25 = 20$ cups of chicken feed. | Wendi feeds each chicken 3 cups of feed per day. She feeds her flock 15 cups of feed in the morning and 25 cups of feed in the afternoon. The total amount of feed she gives her flock is $15 \text{ cups} + 25 \text{ cups} = 40$ cups. Since each chicken gets 3 cups of feed per day, the total number of chickens in her flock is $40 \text{ cups} / 3 \text{ cups} = 13.333333333333333$. | $15 \text{ cups} + 25 \text{ cups} + 10 \text{ cups} = 50$ cups of feed. | 15 cups in the morning + 25 cups in the afternoon = $15 + 25 = 40$ cups of feed. Each chicken gets 3 cups of feed, so 40 cups of feed / 3 cups per chicken = $40 / 3 = 13.33$ chickens. Since there are 20 chickens, the number of cups of feed in the final meal is $20 - 13.33 = 6.67$ cups. | $15 \text{ cups} + 25 \text{ cups} = 40$ cups of feed. 20 chickens x 3 cups = $20 \times 3 = 60$ cups of feed. $60 \text{ cups} - 40 \text{ cups} = 20$ cups of feed. |
| Question: A robe takes 2 bolts of blue fiber and half that much white fiber. How many bolts in total does it take? Answer: | It takes $2 + 1 = 3$ bolts of white fiber. So the total amount of fabric is $2 + 1 = 3$ bolts of fabric. | $2 + 2 = 4$ bolts. | 2 blue bolts + 2 white bolts = $2 + 2 = 4$ bolts in total. | $2 + 1 = 3$ bolts. | $2 + 2 = 4$ bolts. |
| Question: Josh decides to try flipping a house. He buys a house for \$80,000 and then puts in \$50,000 in repairs. This increased the value of the house by 150%. How much profit did he make? Answer: | The cost of the house and repairs came out to $80,000 + 50,000 = 130,000$. He increased the value of the house by $80,000 \times 1.5 = 120,000$. So the new value of the house is $120,000 + 80,000 = 200,000$. So he made a profit of $200,000 - 130,000 = 70,000$. | The house is now worth 150% of \$80,000, which is $80,000 \times 1.5 = 120,000$. So he made $120,000 - 80,000 - 50,000 = 20,000$. | Josh bought the house for \$80,000 and spent \$50,000 on repairs. So he spent $80,000 + 50,000 = 130,000$ on the house. So Josh spent \$130,000 on the house. | Josh bought the house for \$80,000 and put in \$50,000 in repairs. The value of the house increased by 150%, so the new value is $1.5 \times 80,000 + 50,000 = 180,000$. So Josh made $180,000 - 80,000 - 50,000 = 50,000$ in profit. | The value of the house increased by 150%, so it's now 150% of \$80,000, which is \$120,000. Josh spent $80,000 + 50,000 = 130,000$ on the house, so he made $120,000 - 130,000 = -10,000$. |

